Multiferroic Bi_2NiMnO_6 thin films: A computational prediction

Oswaldo Diéguez[1,2] and Jorge Íñiguez[3]

[1]*Department of Materials Science and Engineering, Faculty of Engineering, Tel Aviv University, Tel Aviv 69978, Israel*

[2]*The Raymond and Beverly Sackler Center for Computational Molecular and Materials Science, Tel Aviv University, Tel Aviv 69978, Israel*

[3]*Materials Research and Technology Department, Luxembourg Institute of Science and Technology, 5 avenue des Hauts-Fourneaux, L-4362 Esch/Alzette, Luxembourg*

(Received 26 September 2016; revised manuscript received 20 December 2016; published 21 February 2017)

We report first-principles calculations for one of the few materials that is believed to be a ferroelectric ferromagnet, Bi_2NiMnO_6. Our calculations show that, contrary to what has been reported so far, bulk Bi_2NiMnO_6 does not have a polarization. Instead, like $BiMnO_3$, it crystallizes into a centrosymmetric structure with space group $C2/c$. We also predict that Bi_2NiMnO_6 will indeed be a ferroelectric ferromagnet if it is grown as an epitaxial film on a substrate with in-plane square symmetry and a lattice constant around 4 Å, such as $BaTiO_3$ or $PbZr_{1-x}Ti_xO_3$.

DOI: 10.1103/PhysRevB.95.085129

I. INTRODUCTION

The possibility of manipulating the magnetization of a material by using an electric field is probably the most attractive envisioned application of magnetoelectric multiferroics: ferroelectrics with magnetic ordering [1]. Even if the mechanisms responsible for ferroelectricity and magnetism are somewhat exclusive of each other [2,3], in the last decade a large research effort has gone into searching for these materials [4–16]. This effort has mainly focused on two groups of complex oxides: those in which different species are responsible for the polarization and the magnetism and those in which the magnetic ordering breaks the inversion symmetry of the structure to create a small polarization. $BiFeO_3$ belongs to the first group, and it is by far the most studied multiferroic [17], mainly because it keeps both its ferroic orderings well above room temperature; it is also relatively easy to prepare in bulk and film form, and it has a simple crystal structure, a perovskite in which inversion symmetry is broken to accommodate the lone pair of Bi atoms in the A site, while the B site harbors the Fe ions whose d electrons are responsible for magnetism. However, the ferromagnetic component in $BiFeO_3$ is tiny; instead, the spins of two neighboring Fe ions are almost perfectly antiparallel. In the difficult search for single-phase ferroelectric ferromagnets that would allow for a direct hysteresis loop of magnetization with electric field some candidate materials have been proposed. Examples include $EuTiO_3$ (although ferromagnetism only settles at around 4 K [18]), $LuFe_2O_4$ (although whether this is a ferroelectric is still under debate [19,20]), Fe_3O_4 (although the exact structure that arises below the Verwey transitions is not yet understood [21]), $CoCr_2O_4$ (although both the magnetization and the polarization are very small [22]), and, more recently, the metastable ϵ-Fe_2O_3 [23].

Researchers have also explored perovskite oxides similar to $BiFeO_3$, but with other transition-metal ions instead of Fe. $BiMnO_3$ is the only member of this group that displays strong ferromagnetism. Initial reports attributed a polar $C2$ space group to bulk $BiMnO_3$ [24,25], but more recent studies agree that this is a paraelectric with $C2/c$ symmetry [26–28]. It is possible to change the structure of this material by growing it as an epitaxial thin film, although the calculations of Hatt and Spaldin [29] showed that when the substrate-imposed distortion is small enough to keep the ferromagnetism in $BiMnO_3$, polarization does not develop, and our calculations [30] showed that when the distortion is large enough to create a large polarization, then ferromagnetism turns into antiferromagnetism. Another way to try to modify the properties of these oxides is to add a second species in one of the sites of the perovskite. Azuma and coworkers reasoned that the Goodenough-Kanamori rules [31,32] predict a ferromagnet if Mn and Ni share the sites inside O_6 octahedra in a rocksalt pattern; when they prepared Bi_2NiMnO_6 by high-pressure synthesis, they indeed measured large parallel magnetic moments [33], which persisted up to a Curie temperature of 140 K. After their synchrotron x-ray powder diffraction, they concluded that the material shows a heavily distorted double-perovskite structure where the Ni^{2+} and Mn^{4+} ions are indeed ordered in a rocksalt configuration; they assigned the space group $C2$ to this crystal. Later, first-principles calculations characterized this structure further and quoted a value of the polarization around 20 $\mu C/cm^2$ [34–36].

Unlike those previous studies, our first-principles calculations show that bulk Bi_2NiMnO_6 is actually a paraelectric material with the $C2/c$ space group, the same situation as for $BiMnO_3$. However, we predict that when Bi_2NiMnO_6 films are grown under achievable tensile epitaxial strain, they will indeed become a ferroelectric ferromagnet with a large polarization (70 $\mu C/cm^2$) and a magnetization above 2 μ_B per transition-metal cation, as in the bulk compound [33]. We describe the methodology we have used for our calculations in Sec. II, present our results for the bulk material in Sec. III A and for epitaxial films in Sec. III B, and summarize the implications of our work in Sec. IV.

II. METHODS

Our first-principles calculations are based on density-functional theory (DFT) [37,38] as implemented in the VASP [39] code. In our previous study on $BiMnO_3$ [30] we showed that the Heyd-Scuseria-Ernzerhof hybrid functional of Ref. [40] (HSE06) could sort the different minima of the energy surface of the crystal in a way compatible with experiment (while other DFT-based methods could not). We

have found that this is also the case for Bi_2NiMnO_6. In fact, it has been reported that the HSE06 method predicts band gaps for solids that are very close to experimental results [40], and in particular it performs well for perovskite oxides such as $BiFeO_3$ [41]. Unlike methods that include a Hubbard U, no additional fitting of parameters depending on the material is required in HSE06 (by definition, this method uses a fraction of exact exchange equal to 25% and a range-separation parameter equal to 0.20 $Å^{-1}$).

The main disadvantage of HSE06 is that it is two orders of magnitude slower than standard DFT for our material when using VASP. Therefore, to do initial relaxation steps we used DFT with a Hubbard U and J [42] applied to the d orbitals of Ni^{2+} and Mn^{4+} (we refer to these calculations as DFT+U). We also resorted to this approximation when computing properties for which both methods are known to give similar results (such as whether a crystal structure is a minimum of the energy and what magnetic orderings are favored in a crystal). Based on previous works with perovskite oxides by us and others, including a variety of studies of nickelates [43,44] and manganites [30,43,45], we have chosen the parameters $U_{Ni} = 1$ eV, $J_{Ni} = 0$ eV, $U_{Mn} = 4$ eV, and $J_{Mn} = 1$ eV. However, we also did extensive tests using combinations of $U - J$ equal to values between 0 and 4 eV for Ni and Mn; these tests gave identical results regarding how local minima are ordered in energy [46]. The main variation in the tests is a closing of the band gap as $U - J$ becomes small. However, our tests show that even regular DFT should produce identical results for most of the properties described in this study (as long as the band gap does not spuriously become zero). The values of U and J that we have chosen predict band gaps similar to those computed with HSE06.

We used the Perdew-Burke-Ernzerhof DFT exchange-correlation functional adapted to solids (PBEsol) [47]. To treat the ionic cores we resorted to the projector augmented-wave method [48], solving for the following electrons: Ni and Mn $3p$, $3d$, and $4s$; Bi $5d$, $6s$, and $6p$; and O $2s$ and $2p$. The plane-wave basis set kinetic-energy cutoff was 500 eV. We performed integrations in the Brillouin zone using k-point grids with densities similar to that of the $6 \times 6 \times 6$ mesh for a five-atom perovskite unit cell.

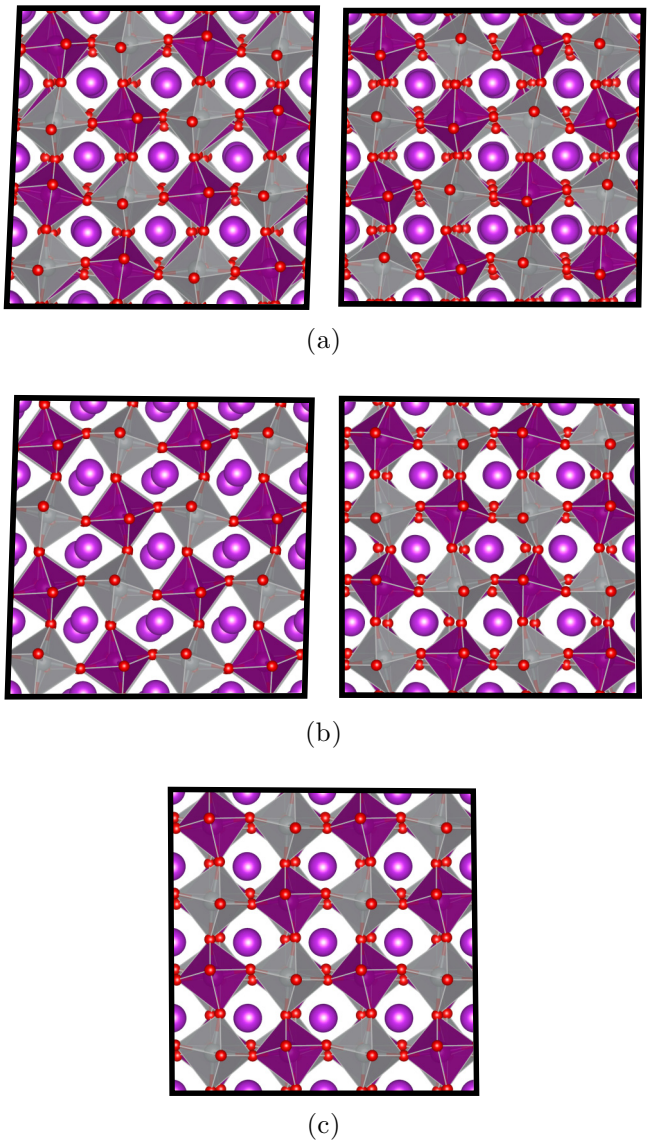

FIG. 1. Inequivalent side views of a pseudocubic unit cell for bulk Bi_2NiMnO_6 structures that correspond to energy minima according to our DFT+U calculations: (a) $C2/c$, (b) $P2_1/n$, and (c) $R3$.

III. RESULTS

A. Bulk phases

Our first set of calculations involves the optimization of Bi_2NiMnO_6 bulk structures that might be competitive in energy with the ground state. As mentioned in the Introduction, previous experimental and computational studies consider that this ground state belongs to the $C2$ space group; Refs. [33,34] report the lattice parameters and Wyckoff positions of the atoms in the crystal unit cell, and we have run optimizations starting from those configurations. In the following we call this structure GS: the structure that the bulk material displays at low temperature and low pressure. Another relevant phase is the one observed at high temperature with space group $P2_1/n$, fully described in Ref. [49]; this phase is analogous to the $Pnma$ phase that appears in many $BiMO_3$ perovskites at high pressure and/or high temperature [50] but with reduced symmetry because of the superimposed rocksalt pattern of Ni^{+2} and Mn^{+4} cations. By analogy with our previous paper about $BiMnO_3$ [30], we call this paraelectric phase p. Based on our previous experience in the search for new phases of $BiFeO_3$ [51], $BiCoO_3$ [52], and $BiMnO_3$ [30], we also relaxed ferroelectric phases similar to the rhombohedral ground state of $BiFeO_3$ (so-called R phases) and to the supertetragonal ground state of $BiCoO_3$ (so-called T phases); we have enforced the same rocksalt cation pattern known to exist in both experimentally characterized phases of Bi_2NiMnO_6. We have optimized these structures using the DFT+U and the HSE06 methods, obtaining similar results with both approaches regarding their structural details. The atomic structure of the resulting optimized structures (with forces converged below 0.015 eV/Å and stress components below 0.1 GPa) is shown in Fig. 1, while Table I contains the values of several magnitudes of interest for these phases.

TABLE I. Properties of Bi_2NiMnO_6 phases that are local energy minima according to our calculations (with DFT+U and HSE06) and comparison with experiment (from Refs. [33,49]). We report the space group, lattice parameters, lattice angles, Wyckoff positions, polarization P, and energy difference with the GS phase ΔE. GS, p, and R label the ground-state phase, the high-temperature paraelectric phase, and the R rhombohedral phase found in this study, respectively.

Phase	Properties	DFT+U	HSE06	Expt.
GS	Space group	$C2/c$	$C2/c$	$C2$
	a (Å)	9.3871	9.3523	9.4646
	b (Å)	5.3739	5.3558	5.4230
	c (Å)	9.5355	9.4679	9.5431
	β (°)	107.64	107.66	107.82
	Mn 1	(0.2500,0.2500,0.0000)	(0.2500,0.2500,0.0000)	(0.257,0.250,0.001)
	Ni 1	(0.0000,0.2648,0.2500)	(0.0000,0.2609,0.2500)	(0.000,0.252,0.250)
	Ni 2			(0.000,0.737,0.750)
	Bi 1	(0.6308,0.2323,0.1235)	(0.6314,0.2230,0.1248)	(0.633,0.214,0.128)
	Bi 2			(0.631,0.772,0.627)
	O 1	(0.5897,0.1970,0.5833)	(0.5914,0.1949,0.5823)	(0.611,0.176,0.599)
	O 2	(0.1582,0.0385,0.3860)	(0.1602,0.0344,0.3860)	(0.146,0.013,0.386)
	O 3	(0.3498,0.0350,0.1577)	(0.3493,0.0374,0.1565)	(0.333, − 0.021,0.163)
	O 4			(0.920,0.279,0.430)
	O 5			(0.377,0.941,0.649)
	O 6			(0.662,0.453,0.876)
	P (μC/cm^2)	0	0	N/A
	ΔE (meV/f.u.)	0	0	
p	Space group	$P2_1/n$	$P2_1/n$	$P2_1/n$
	a (Å)	5.3590	5.3182	5.4039
	b (Å)	5.5522	5.5262	5.5668
	c (Å)	7.6517	7.6007	7.7330
	β (°)	90.00	90.00	90.166
	Mn 1	(0.0000,0.5000,0.0000)	(0.0000,0.5000,0.0000)	(0.0000,0.5000,0.0000)
	Ni 1	(0.5000,0.0000,0.0000)	(0.5000,0.0000,0.0000)	(0.5000,0.0000,0.0000)
	Bi 1	(0.0086,0.0549,0.2509)	(0.0072,0.0553,0.2512)	(0.0049,0.0468,0.2510)
	O 1	(0.3067,0.2878,0.4589)	(0.3109,0.2860,0.4589)	(0.280,0.279,0.477)
	O 2	(0.2921,0.3040,0.0386)	(0.2907,0.3080,0.0380)	(0.281,0.281,0.053)
	O 3	(0.58372 − 0.0222,0.2556)	(0.5851, − 0.0238,0.2583)	(0.594, − 0.022,0.252)
	P (μC/cm^2)	0	0	0
	ΔE (meV/f.u.)	−30	24	
R	Space group	$R3$	$R3$	
	a (Å)	5.4526	5.4428	
	α (°)	60.35	60.02	
	Mn 1	(0.7250,0.7250,0.7250)	(0.7208,0.7208,0.7208)	
	Ni 1	(0.2284,0.2284,0.2284)	(0.2255,0.2255,0.2255)	
	Bi 1	(0.0000,0.0000,0.0000)	(0.0000,0.0000,0.0000)	
	Bi 2	(0.4985,0.4985,0.4985)	(0.4987,0.4987,0.4987)	
	O 1	(0.4114, − 0.0566,0.5483)	(0.4122, − 0.0646,0.5450)	
	O 2	(0.0330,0.4609, − 0.0967)	(0.0225,0.4580, − 0.1000)	
	P (μC/cm^2)	70	79	
	ΔE (meV/f.u.)	−4	17	

The main results from Table I are that (i) our attempts to optimize the polar $C2$ phase always ended up in a nonpolar structure with $C2/c$ space group, (ii) our PBSsol+U and HSE06 methods give different predictions regarding which phase is the ground state of bulk Bi_2NiMnO_6, (iii) there is a ferromagnetic R phase with large polarization that is competitive with the phases known so far to exist, and (iv) no T phase is obtained as a result of our optimizations. In the following, we provide more details about each of these points.

First, we tackle the issue of the ground state of bulk Bi_2NiMnO_6; our computational result is different from the experimental result. When DFT-based methods predict a ground state of a crystal that is different from the one obtained experimentally, it usually happens that the computational method finds more than one competitive minimum in a small range of energies. DFT-based methods require approximations for the exchange-correlation potential, and there are errors in these approximations, so some functionals might favor a structure that is not the actual ground state. An example of this occurs in crystalline iron, where the fcc structure is very close in energy to the bcc structure, so little differences in methodology details might favor one over the other [53],

but both structures are local minima of the energy. The case described here for Bi_2NiMnO_6 is different: only the $C2/c$ structure is a minimum of the energy according to every DFT-based method we have tried. This includes calculations in which we used the PBE exchange-correlation potential [54] instead of PBEsol, calculations in which we fixed the lattice vectors to the experimental values reported in Ref. [33], calculations for different values of $U - J$ (as described in Sec. II), and calculations in which spin-orbit coupling was taken into account. Every structure we have set up with the $C2$ space group lowered its energy when the atoms were allowed to move, ending always in a $C2/c$ structure like the one displayed in Fig. 1(a). Structurally, this $C2/c$ phase is not very different from the experimental $C2$ structure, as shown by the Wyckoff positions and lattice parameters in Table I; however, the two critically differ in that only in the $C2/c$ case do the off-center displacements of the Bi ions compensate each other to give a centrosymmetric structure (in this sense, Bi_2NiMnO_6 resembles an antiferroelectric).

So why was the $C2/c$ structure missed in the experimental study of Ref. [33]? At the time, the parent compound $BiMnO_3$ was believed to belong to space group $C2$, so it was reasonable to fit the results of diffraction for Bi_2NiMnO_6 to that space group. Only later did both experiment and computations agree that the space group of $BiMnO_3$ is $C2/c$ instead of $C2$ [26–28]. Hence, probably due to this chronology, a fit to the $C2/c$ structure has not yet been tried in the case of Bi_2NiMnO_6.

Further support for the centrosymmetric $C2/c$ structure is given by two facts. First, no experimental measurement of the polarization has been reported for bulk Bi_2NiMnO_6 (only theoretical values have been quoted using point-charge models or Berry-phase first-principles theory [33–36,55]). Second, the reported $C2$ structure contains two different environments for the Ni^{2+} ions and one for the Mn^{+4} ions, but there is no explanation so far for this; there are no signs of charge or orbital ordering, for example. In the $C2/c$ structure, the environment of every Ni ion is the same, which is also the case for every Mn ion.

We must also mention that there is one instance of previous first-principles calculations [34] that did report that a $C2$ phase was found after optimization (albeit with quite different Wyckoff positions than the experimental work). We have tried to reproduce those calculations using a methodology similar to that of Ref. [34], but by allowing enough relaxation steps the optimized structure slowly converged to the $C2/c$ one presented here. Again, we must bear in mind that at the time of those calculations, the $C2/c$ phase was unknown, so it was not considered explicitly in this study. Our calculations show that an optimization that starts with a $C2$ space group will arrive at the $C2/c$ space group minima only if a demanding threshold for the forces is used (less than 0.001 eV/Å). In the absence of information about the possible existence of a $C2/c$ phase, otherwise sensible thresholds of around 0.01 eV/Å will fail to reveal the centrosymmetric phase. Other first-principles studies of Bi_2MnNiO_6 were done fixing the structure either to the experimental one [35,55] or to the relaxed first-principles one of Ciucivara and coworkers [36].

To add to the puzzle of the possible paraelectricity of bulk Bi_2NiMnO_6, a sizable polarization has indeed been measured in Bi_2NiMnO_6 *films*. The group that synthesized this double perovskite for the first time in bulk also grew it as a film on $SrTiO_3$ using pulsed laser deposition [56]. They measured a polarization of 5 $\mu C/cm^2$ and a magnetic Curie temperature of 100 K. Their films displayed a pseudotetragonal structure with $a = b = 3.91$ Å (matching the substrate) and $c = 3.87$ Å, described as rather different from the bulk one, while keeping the same rocksalt pattern [57]. Using a chemical solution deposition method, Lai *et al.* [58] grew Bi_2NiMnO_6 films with and without $SrTiO_3$ buffer layers on a $Pt(111)/Ti/SiO_2/Si(100)$ substrate, obtaining polarizations around 6 and 8 $\mu C/cm^2$. Again, the situation can be compared to that of $BiMnO_3$, where polarizations between 9 and 23 $\mu C/cm^2$ have been reported for films [59–61] even if the bulk is nonpolar. For $BiMnO_3$ we proposed that those measurements might be related to the formation of film phases under strain that are polar [30], and this might also be the case in Bi_2NiMnO_6 films.

We move on now to the issue of the predicted ground state by different methodologies. Table I shows that the three local minima of the energy surface of Bi_2NiMnO_6 lie within only 30 meV per formula unit (five-atom group of the standard perovskite unit cell; in our case, $BiNi_{1/2}Mn_{1/2}O_3$). Our DFT+U method predicts a higher energy for the GS phase than for the other two (this does not change when we explore different values of U as described in Sec. II; in particular, the energy difference between the GS and p phases changes only between 29 and 39 meV/f.u. in that range of $U - J$ values). This happened too for $BiMnO_3$ [30], where the situation is corrected by the HSE06 hybrid. We have shown in the past that different exchange-correlation functionals predict almost the same minima of the energy surface of $BiMnO_3$ [30] and $BiFeO_3$ [51], although how those minima are ordered in energy can vary from functional to functional. As for Bi_2NiMnO_6, here we use the fast DFT+U method when we are interested in finding possible energy minima or when we are interested in energy differences between very similar structures, while we will resort to the more accurate and slow HSE06 when it is important to evaluate energy differences between different phases.

Both DFT+U and HSE06 predict that there exists a metastable ferromagnetic rhombohedral structure with a polarization around 70 $\mu C/cm^2$ when computed using the Berry-phase formalism (we have checked that typical antiferromagnetic alignments are higher in energy; details are given later for similar films). This is a structure like that of bulk $BiFeO_3$ but where the superimposed rocksalt pattern of Mn^{4+} and Ni^{2+} causes a reduction from the $R3c$ space group to the $R3$ symmetry; it is represented in Fig. 1(c). According to first-principles calculations, a similar structure is also metastable for $BiCoO_3$ [52] and $BiMnO_3$ [30].

Regarding the electronic structure, the GS, p, and R phases display similar density-of-states profiles, as shown in Fig. 2 (this was also the case for different phases in $BiFeO_3$ [51]). The band gap in all cases is around 1 eV.

Unlike in $BiCoO_3$, $BiFeO_3$, and $BiMnO_3$, no T structures appeared as local minima of the energy in our Bi_2NiMnO_3 search. We relaxed variations of the T configurations of those other materials with the added rocksalt pattern of Mn^{4+} and Ni^{2+}, but the resulting structure was always one of the other three local minima. When trying to favor a T structure, we found that the material uses the extra freedom of having two

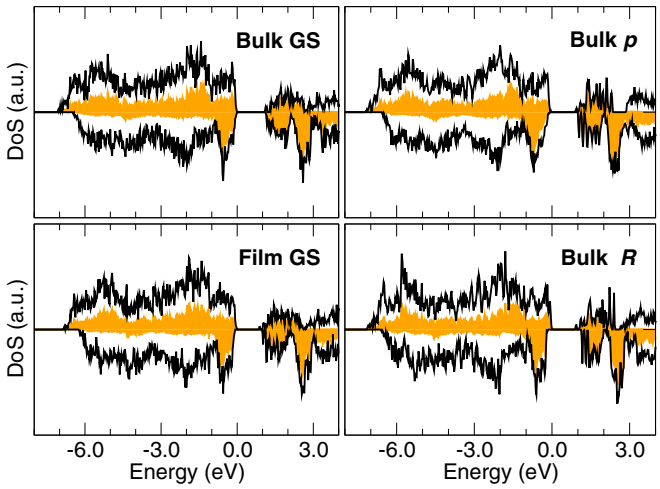

FIG. 2. DFT+U density of states for the three bulk phases that are local minima of the energy and for the GS epitaxial film at an in-plane lattice parameter of 4 Å. The lines represent the total density of states, and the shaded areas correspond to its projection onto the d orbitals of Ni and Mn (hybridized mostly with the p orbitals of O).

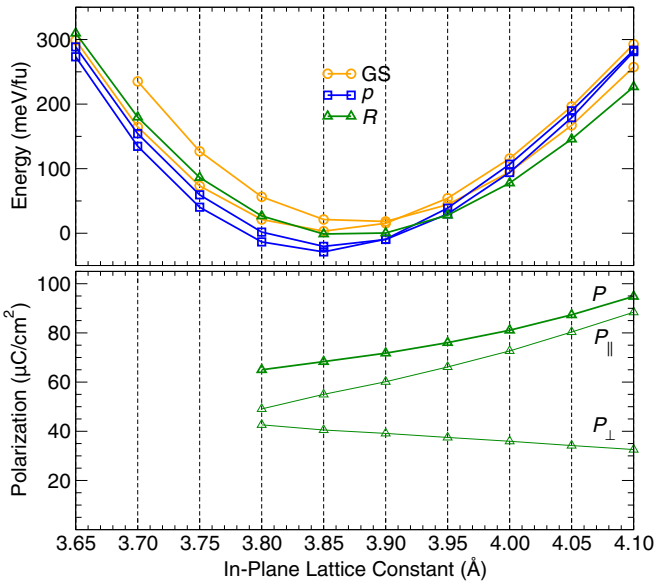

FIG. 3. Top: DFT+U energy of relaxed (001) films as a function of the in-plane lattice parameter; the films are adaptations of the bulk GS (two possible orientations), p (two possible orientations), and R (one inequivalent orientation) phases to the mechanical boundary conditions imposed by the square symmetry of the substrate. Bottom: magnitude of the polarization of the R films (P), its component on the film ($P_{||}$), and its component perpendicular to the film ($P_{\perp}$).

different cations inside the O_6 octahedra to distort those two environments in ways that allow the other phases to survive in regimes of large compressive strain where oxides such as $BiMnO_3$ transition to a T phase [30].

B. Epitaxial films

One possible way to stabilize a metastable phase of the bulk of a material is to grow it as a thin film on a substrate. In this way, the epitaxial misfit strain acts as a handle to vary the relative energies of the possible bulk phases; it is then a matter of assessing, either by computation or by experiment, whether a particular phase of a film will be the most stable one under those strain conditions [62]. We have simulated coherent epitaxial (001) films of Bi_2NiMnO_3 by doing calculations of the bulk material in which we impose mechanical boundary conditions determined by the lattice constant of the substrate, assumed to display in-plane square symmetry (this is indeed the case for many perovskite substrates cut perpendicularly to one of the principal axes).

As a starting point, we adapted the three bulk phases described in the previous section to the in-plane square symmetry. There are two inequivalent ways to do this for the GS and p phases and one way for the R phase, as shown in Fig. 1. This causes small distortions that make the in-plane lattice vectors form a 90° angle and have the same magnitude (in the adapted p and R phases) or a ratio of magnitudes equal to 2 (in the GS phase). In all cases, those distortions cost only a few meV per formula unit. Then, we do calculations in which we expand or contract the lattice vectors to mimic the effect of squared substrates with different lattice constants. We do this in intervals of 0.05 Å, and we use the Wyckoff positions and out-of-plane lattice vector of the previous geometry as a starting point of the next geometry relaxation. In this way, we arrive at a graphic of the energy of the films as a function of the in-plane lattice constant that we show in Fig. 3 (top). These calculations were done using the DFT+U method.

For strains around the minimum of the energy curves the adopted configuration is paraelectric. However, for high enough tensile strains the R phase has lower energy than the other phases. These strains correspond to in-plane lattice constants of the order of 4 Å, so this phase is expected to appear if the films are grown over perovskite oxides such as $BaTiO_3$ and $PbZr_{1-x}Ti_xO_3$ (PZT). Figure 3 (bottom) shows that the computed polarization of the films is similar to the 70 $\mu C/cm^2$ of the bulk phase. The electronic structure of the films is very similar to that of the bulk, as illustrated in Fig 2 for the film with in-plane lattice parameter $a = 4$ Å.

All GS, p, and R films at tensile epitaxial strains have magnetic cations with magnetic moments around 3 μ_B for Mn^{4+} and around 2 μ_B for Ni^{2+}. Figure 4(a) shows that below in-plane lattice parameters around 4.05 Å ferromagnetism prevails over the alternative antiferromagnetic (AFM) orderings typical of perovskites: G type (first-nearest-neighbor spins antiferromagnetically aligned), C type (parallel spin alignment along the out-of-plane, perpendicular-to-the-substrate direction and antiparallel alignment in plane), C′ type (parallel spins along a direction in the plane of the substrate and antiparallel in the perpendicular plane), A type (ferromagnetism in plane and antiparallel alignment out of plane), and A′ type (antiparallel alignment along a direction in the plane of the substrate and parallel alignment in the perpendicular plane). This is not surprising since the network of transition-metal ions and oxygen atoms connecting them has angles and bond lengths similar to those of the bulk network, known to be ferromagnetic.

Following a prescription we have described in earlier articles [30,52,63], we have used the DFT+U energy differences

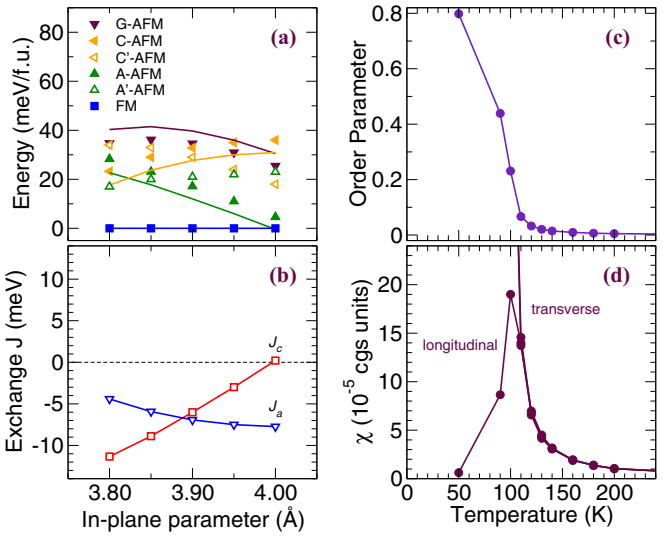

FIG. 4. Magnetic properties of R films: (a) DFT+U values of the energy of different magnetic arrangements (symbols) and fit to a Heisenberg model (lines; we have used the configurations marked with solid symbols for this fit), (b) exchange coupling constants J that result from this fit, (c) ferromagnetic order parameter as a function of temperature obtained from the Heisenberg model when $a = 3.95$ Å, and (d) longitudinal and transverse magnetic susceptibility obtained from the Heisenberg model when $a = 3.95$ Å.

between ferromagnetic (FM), A-AFM, C-AFM, and G-AFM magnetic arrangements to fit a simplified Heisenberg model. This model has as parameters two exchange constants, J_a and J_c, that take into account the strength of the magnetic interaction between neighboring Ni-Mn pairs in plane and out of plane, respectively; their values are represented in Fig. 4(b). A Monte Carlo method on a lattice of $20 \times 20 \times 20$ spins was used with this Heisenberg model to study the behavior of the magnetic ordering with temperature. Doing this, we found that the ferromagnetic order parameter takes values other than zero for temperatures below a Curie point of around 100 K, as shown in Fig. 4(c); this is in agreement with experimental measurements done in Bi_2NiMnO_3 films [56]. The magnetic susceptibility computed from the Monte Carlo simulations with this Heisenberg model is plotted in Fig. 4(d).

The results for films presented so far were obtained using DFT+U calculations. As for $BiMnO_3$ [30], this methodology does not resolve the close energy differences between phases in agreement with experiment, but the HSE06 hybrid functional does. When we applied it to do computations for tensile films of Bi_2NiMnO_6, it also predicted that the R phase is the most stable one for large enough strains, as shown in Fig. 5.

In order to further explore the energy surface of bulk Bi_2NiMnO_6 in the search of minima that might be relevant in films, we did one more set of calculations. We took every film structure represented by a point in Fig. 3, removed the epitaxial constraints, performed a few steps of molecular dynamics to allow it to explore its surroundings, and relaxed this structure until the forces and stresses were almost zero. During this annealing process the atoms visited structures that were up to a few eV/f.u. higher in energy than the ground state. By the end of the search, most of the initial structures had

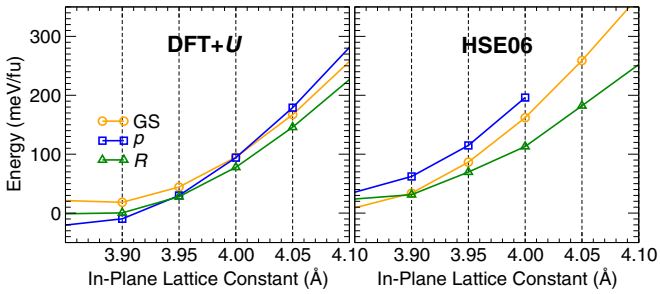

FIG. 5. Comparison of the energy of relaxed films as a function of the in-plane lattice parameter when using DFT+U (left) and HSE06 (right). When two orientations of the films are possible (GS and p phases), we have done HSE06 calculations for the one with lowest DFT+U energy in most of the range of in-plane lattice parameters.

converged to a configuration with forces below 0.015 eV/Å, and these are represented in Fig. 6, where the energy with respect to the bulk ground state is plotted as a function of the average of the two closest in-plane lattice constants of the optimized structure. We see that the low-energy points are near the minima of the film curves in Fig. 3, showing that in several cases releasing the epitaxial constraints just takes the system to one of the three bulk phases described in this work. After analyzing the rest of the crosses in Fig. 6, it turns out that they also correspond to one of the GS, p, or R phases, but with a different electronic configuration (e.g., the value at around 550 meV/f.u. is an R structure where all ions show zero magnetic moments). Overall, we are confident that no other low-energy structures exist for typical in-plane lattice constants, particularly in the region where the films are found to be ferroelectric and ferromagnetic.

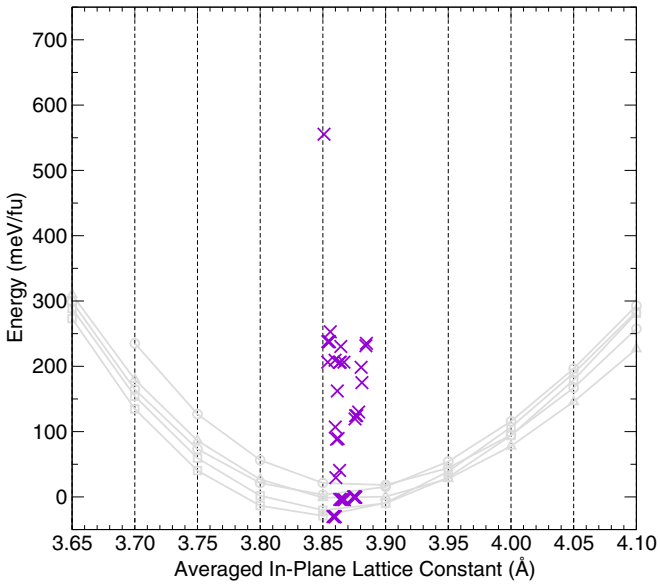

FIG. 6. The crosses correspond to the energy of the bulk optimized structures that result after performing an annealing on each of the film structures recorded in Fig. 3 as described in the text. In gray we have copied the data of Fig. 3 for reference.

IV. SUMMARY AND CONCLUSIONS

Our first-principles calculations for bulk Bi_2NiMnO_6 are consistent with a nonpolar crystal structure of space group $C2/c$. Previous reports pointed to a $C2$ polar space group, but the reasons stated in Sec. III A lead us to believe that, like what happened with $BiMnO_3$, this is not correct.

Our calculations also show that when Bi_2NiMnO_6 is grown on a (001)-oriented perovskite substrate of materials such as $BaTiO_3$ and PZT the epitaxial strain should favor a phase that is both ferroelectric and ferromagnetic. The polarization of these films is around 70 $\mu C/cm^2$, similar to that of the most used ferroelectric materials. The films are predicted to be ferromagnetic with magnetic moments of 2.5 μ_B per formula unit and a Curie temperature of around 100 K. Thus, our simulations predict that, in thin-film form, Bi_2NiMnO_6 is one of the very few known magnetoelectric multiferroics with a strong ferromagnetic order.

ACKNOWLEDGMENTS

O.D. acknowledges funding from the Israel Science Foundation through Grants No. 1814/14 and No. 2143/14. J.Í. was financially supported by the Luxembourg National Research Fund through the Pearl (Grant No. P12/485315) and Core (Grant No. C15/MS/10458889) programs.

[1] M. Bibes and A. Barthélémy, Nat. Mater. **7**, 425 (2008).
[2] N. A. Hill, J. Phys. Chem. B **104**, 6694 (2000).
[3] S. Bhattacharjee, E. Bousquet, and P. Ghosez, Phys. Rev. Lett. **102**, 117602 (2009).
[4] M. Fiebig, J. Phys. D **38**, R123 (2005).
[5] W. Prellier, M. P. Singh, and P. Murugavel, J. Phys. Condens. Matter **17**, R803 (2005).
[6] D. I. Khomskii, J. Magn. Magn. Mater. **306**, 1 (2006).
[7] W. Eerenstein, N. D. Mathur, and J. F. Scott, Nature (London) **442**, 759 (2006).
[8] C. N. R. Rao and C. R. Serrao, J. Mater. Chem. **17**, 4931 (2007).
[9] R. Ramesh and N. A. Spaldin, Nat. Mater. **6**, 21 (2007).
[10] Y. Tokura, J. Magn. Magn. Mater. **310**, 1145 (2007).
[11] S. W. Cheong and M. Mostovoy, Nat. Mater. **6**, 13 (2007).
[12] C.-W. Nan, M. I. Bichurin, S. Dong, D. Viehland, and G. Srinivasan, J. Appl. Phys. **103**, 031101 (2008).
[13] K. F. Wang, J.-M. Liu, and Z. F. Ren, Adv. Phys. **58**, 321 (2009).
[14] A. R. Akbashev and A. R. Kaul, Russ. Chem. Rev. **80**, 1159 (2011).
[15] J. Ma, J. Hu, Z. Li, and C.-W. Nan, Adv. Mater. **23**, 1062 (2011).
[16] A. P. Pyatakov and A. K. Zvezdin, Phys. Usp. **55**, 557 (2012).
[17] G. Catalan and J. F. Scott, Adv. Mater. **21**, 2463 (2009).
[18] J. H. Lee, L. Fang, E. Vlahos, X. Ke, Y. W. Jung, L. F. Kourkoutis, J.-W. Kim, P. J. Ryan, T. Heeg, M. Roeckerath, V. Goian, M. Bernhagen, R. Uecker, P. C. Hammel, K. M. Rabe, S. Kamba, J. Schubert, J. W. Freeland, D. A. Muller, C. J. Fennie, P. Schiffer, V. Gopalan, E. Johnston-Halperin, and D. G. Schlom, Nature (London) **466**, 954 (2010).
[19] M. Angst, Phys. Status Solidi RRL **7**, 383 (2013).
[20] I. K. Yang, J. Kim, S. H. Lee, S.-W. Cheong, and Y. H. Jeong, Appl. Phys. Lett. **106**, 152902 (2015).
[21] J. van den Brink and D. I. Khomskii, J. Phys. Condens. Matter **20**, 434217 (2008).
[22] Y. Yamasaki, S. Miyasaka, Y. Kaneko, J.-P. He, T. Arima, and Y. Tokura, Phys. Rev. Lett. **96**, 207204 (2006).
[23] M. Gich, I. Fina, A. Morelli, F. Sánchez, M. Alexe, J. Gàzquez, J. Fontcuberta, and A. Roig, Adv. Mater. **26**, 4645 (2014).
[24] T. Atou, H. Chiba, K. Ohoyama, Y. Yamaguchi, and Y. Syono, J. Solid State Chem. **145**, 639 (1999).
[25] A. Moreira dos Santos, A. K. Cheetham, T. Atou, Y. Syono, Y. Yamaguchi, K. Ohoyama, H. Chiba, and C. N. R. Rao, Phys. Rev. B **66**, 064425 (2002).
[26] A. A. Belik, S. Iikubo, T. Yokosawa, K. Kodama, N. Igawa, M. Azuma, M. Takano, K. Kimoto, Y. Matsui, and E. Takayama-Muromachi, J. Am. Chem. Soc. **129**, 971 (2007).
[27] E. Montanari, G. Calestani, L. Righi, E. Gilioli, F. Bolzoni, K. S. Knight, and P. G. Radaelli, Phys. Rev. B **75**, 220101 (2007).
[28] P. Baettig, R. Seshadri, and N. A. Spaldin, J. Am. Chem. Soc. **129**, 9854 (2007).
[29] A. J. Hatt and N. A. Spaldin, Eur. Phys. J. B **71**, 435 (2009).
[30] O. Diéguez and J. Íñiguez, Phys. Rev. B **91**, 184113 (2015).
[31] J. B. Goodenough, J. Phys. Chem. Solids **6**, 287 (1958).
[32] J. Kanamori, J. Phys. Chem. Solids **10**, 87 (1959).
[33] M. Azuma, K. Takata, T. Saito, S. Ishiwata, Y. Shimakawa, and M. Takano, J. Am. Chem. Soc. **127**, 8889 (2005).
[34] A. Ciucivara, B. Sahu, and L. Kleinman, Phys. Rev. B **76**, 064412 (2007).
[35] H. J. Zhao, X. Q. Liu, and X. M. Chen, AIP Adv. **2**, 022115 (2012).
[36] H. J. Zhao and X. M. Chen, AIP Adv. **2**, 042143 (2012).
[37] P. Hohenberg and W. Kohn, Phys. Rev. **136**, B864 (1964).
[38] W. Kohn and L. J. Sham, Phys. Rev. **140**, A1133 (1965).
[39] G. Kresse and J. Furthmuller, Phys. Rev. B **54**, 11169 (1996); G. Kresse and D. Joubert, *ibid.* **59**, 1758 (1999).
[40] A. V. Krukau, O. A. Vydrov, A. F. Izmaylov, and G. E. Scuseria, J. Chem. Phys. **125**, 224106 (2006).
[41] A. Stroppa and S. Picozzi, Phys. Chem. Chem. Phys. **12**, 5405 (2010).
[42] A. I. Liechtenstein, V. I. Anisimov, and J. Zaanen, Phys. Rev. B **52**, R5467 (1995).
[43] M. Gibert, P. Zubko, R. Scherwitzl, J. Íñiguez, and J.-M. Triscone, Nat. Mater. **11**, 195 (2012).
[44] J. Varignon, M. N. Grisolia, J. Íñguez, A. Barthélémy, and M. Bibes, arXiv:1603.05480.
[45] J. Hong, A. Stroppa, J. Íñiguez, S. Picozzi, and D. Vanderbilt, Phys. Rev. B **85**, 054417 (2012).
[46] To perform our tests we used the simplified approach described by S. L. Dudarev, G. A. Botton, S. Y. Savrasov, C. J. Humphreys, and A. P. Sutton, Phys. Rev. B **57**, 1505 (1998).
[47] J. P. Perdew, A. Ruzsinszky, G. I. Csonka, O. A. Vydrov, G. E. Scuseria, L. A. Constantin, X. Zhou, and K. Burke, Phys. Rev. Lett. **100**, 136406 (2008).

[48] P. E. Blöchl, Phys. Rev. B **50**, 17953 (1994)
[49] K. Takata, M. Azuma, Y. Shimakawa, and M. Takano, J. Jpn. Soc. Powder Powder Metall. **52**, 913 (2005).
[50] A. A. Belik, J. Solid State Chem. **195**, 32 (2012).
[51] O. Diéguez, O. E. González-Vázquez, J. C. Wojdeł, and J. Íñiguez, Phys. Rev. B **83**, 094105 (2011).
[52] O. Diéguez and J. Íñiguez, Phys. Rev. Lett. **107**, 057601 (2011).
[53] H. J. F. Jansen and S. S. Peng, Phys. Rev. B **37**, 2689 (1988).
[54] J. P. Perdew, K. Burke, and M. Ernzerhof, Phys. Rev. Lett. **77**, 3865 (1996).
[55] Y. Uratani, T. Shishidou, F. Ishii, and T. Oguchi, Physica B (Amsterdam, Neth.) **383**, 9 (2006).
[56] M. Sakai, A. Masuno, D. Kan, M. Hashisaka, K. Takata, M. Azuma, M. Takano, and Y. Shimakawa, Appl. Phys. Lett. **90**, 072903 (2007).
[57] Y. Shimakawa, D. Kan, M. Kawai, M. Sakai, S. Inoue, M. Azuma, S. Kimura, and O. Sakata, Jpn. J. Appl. Phys. **46**, L845 (2007).
[58] J. L. Lai, X. G. Tang, C. B. Ma, R. Li, Q. X. Liu, and Y. P. Jiang, Integr. Ferroelectr. **139**, 26 (2012).
[59] H. Jeen, G. Singh-Bhalla, P. R. Mickel, K. Voigt, C. Morien, S. Tongay, A. F. Hebard, and A. Biswas, J. Appl. Phys. **109**, 074104 (2011).
[60] J. Y. Son and Y.-H. Shin, Appl. Phys. Lett. **93**, 062902 (2008).
[61] G. M. De Luca, D. Preziosi, F. Chiarella, R. D. Capua, S. Gariglio, S. Lettieri, and M. Salluzzo, Appl. Phys. Lett. **103**, 062902 (2013).
[62] D. G. Schlom, L.-Q. Chen, C. J. Fennie, V. Gopalan, D. A. Muller, X. Pan, R. Ramesh, and R. Uecker, MRS Bull. **39**, 118 (2014).
[63] C. Escorihuela-Sayalero, O. Diéguez, and J. Íñiguez, Phys. Rev. Lett. **109**, 247202 (2012).